Modelling nasal airflow coefficients: an insight into the nature of airflow*

Graham O'Neill, Neil Samuel Tolley

Department of Otolaryngology, Head and Neck Surgery, St Mary's Hospital, London, United Kingdom

Rhinology 59: 1, 66 - 74, 2021
https://doi.org/10.4193/Rhin19.440

***Received for publication:**
December 6, 2019
Accepted: May 26, 2020

Abstract

Background: There has been considerable discussion and conflicting views regarding the presence of laminar or turbulent flow within the nose. The aim of this study was to investigate how the modelling of variable flow coefficients can assist in the evaluation of the characteristics of flow in the resistive segments of the nose.

Methodology: A comparison was made between the flow coefficient for the nasal valve, obtained from a mathematical model, and resistive flow components such as a Venturi meter and orifice tube. Also, a variable loss coefficient was formulated for the whole (unilateral) nose which, by utilising the intersection of the laminar and turbulent asymptotes, provided an estimation for the critical Reynolds number (R_{crit}).

Results: The results show that the flow resistance of the nasal valve is considerably greater than that for both a Venturi meter and an orifice tube implying turbulent or turbulent-like flow for much of nasal inspiration. Regarding the loss coefficient for the whole (unilateral) nose, normal respiration flowrates are displaced well away from the laminar asymptote. The critical Reynolds number was estimated to be 450.

Conclusions: A novel method of determining the flow characteristics of the nose, particularly the critical Reynolds number, is presented. The analysis indicates a higher degree of turbulence than is assumed from a simple traditional calculation using a hydraulic diameter and flow through straight tubes. There are implications for computational fluid dynamics (CFD) modelling where either the entire nasal airflow is assumed to be laminar or a low turbulence model implemented.

Key words: computational fluid dynamics, critical Reynolds number, nasal modelling, nasal valve, unsteady flow

Introduction

Given the air conditioning function of the nose, the inspiratory airflow route through the nose and the degree of turbulence are important considerations. For example, abnormal flow has been associated with atrophic rhinitis, empty nose syndrome, turbinoplasty and rhinosinusitis with nasal polyposis [36, 55-57]. Regarding

Nomenclature: A: Cross sectional flow area; C_d: Flow coefficient (discharge coefficient) = actual flowrate/theoretical flowrate; $K_{L\text{-}turbinate}$: Loss coefficient for the turbinate region; $K_{L\text{-}nose}$: Loss coefficient for the whole (unilateral) nose; *L, k, srt*: Constants associated with the Logistic function used to model the discharge coefficient C_d for the nasal valve (Table 1). *Δp*: Transnasal pressure drop; *Q*: Volumetric flowrate; Re: Reynolds number = ratio of inertial forces to viscous forces; Re_{crit}: Critical Reynolds number (Reynolds number associated with laminar/turbulent transition); *ST, mag, Adj*: Constants associated with the tanh function used to model the loss coefficient for the turbinate region ($K_{L\text{-}turbinate}$); u: Mean fluid velocity; ρ: Density; ν: Kinematic viscosity; μ: Dynamic viscosity; λ, ξ: Coefficients associated with the linear and non-linear terms of the polynomial curve fit of the rhinomanometric data for the whole (unilateral) nose (equation 1). Whilst an explanation of some fluid mechanics terms has been incorporated into the Introduction, some readers may desire a more detailed coverage of elementary theory. If so, we recommend the first half of reference [54].

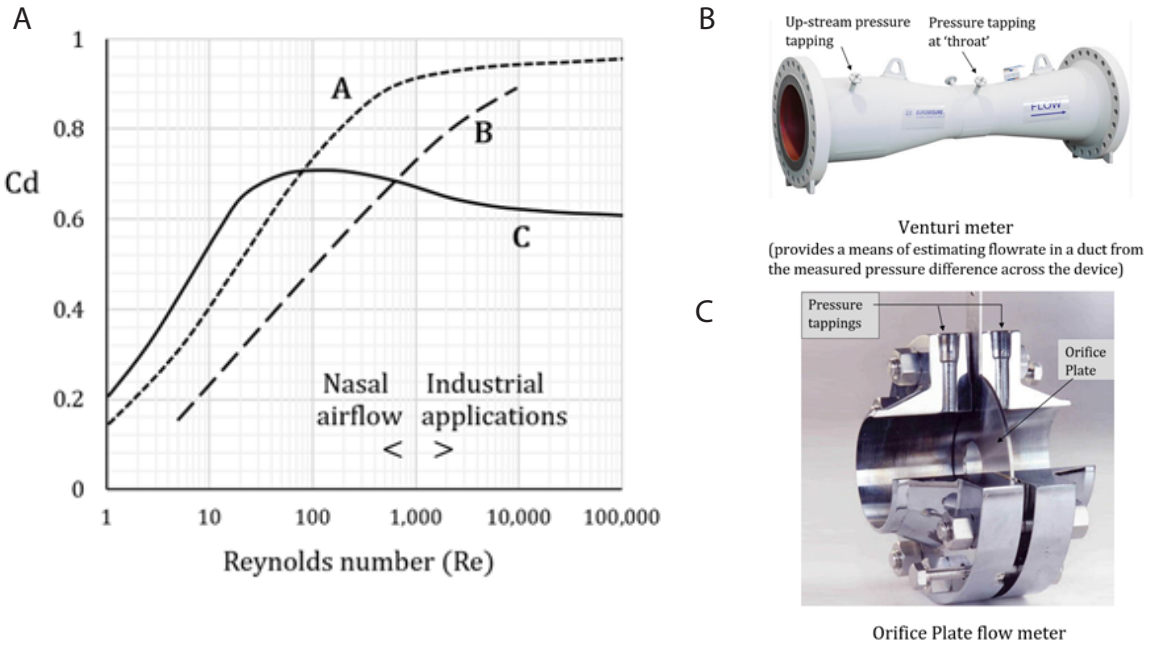

Figure 1. Discharge coefficient C_d as a function of the Reynolds number for A) Venturi meter, B) orifice tube (cylindrical choke) and C) orifice plate.

a theoretical analysis of the nasal pressure -v- flow data, there have been several mathematical models which have utilised Bernoulli's equation with the incorporation of a discharge coefficient, similar to the treatment of flow through a Venturi meter or orifice restriction [1-3]. The discharge coefficient (C_d) is simply a measure of how efficiently a flow component passes a given 'real' fluid compared to an 'ideal' fluid; the latter being incompressible and having no viscosity. Since the discharge coefficient is the ratio of the 'actual' to the 'theoretical' flowrate, then an efficient flow component, such as a Venturi meter, has a discharge coefficient close to 1.0 and a relatively small pressure loss compared to a less efficient component such as an orifice plate (Figure 1). However, for the nose, a significant pressure loss is not necessarily an indication of inefficiency since it is associated with increased mixing of the inspiratory airstream which aids air conditioning. Arguably, over-zealous surgery which results in a very low transnasal pressure drop may not be the most optimal solution for the patient.

The fact that the flow coefficient is dependent upon the prevailing Reynolds number, particularly at low flowrates, has received limited attention. The Reynolds number (Re) is dimensionless being the ratio of inertial forces to viscous forces. It is directly proportional to the fluid velocity such that a lower flowrate will result in a lower Reynolds number, reflecting an increasing influence of viscous forces. For steady flow in long straight pipes, at Reynolds numbers below about 2,000 viscous forces become increasingly important. The effect is to inhibit turbulence with the flow transitioning to become more laminar in character.

For complex geometries there is more disruption of the flow such that turbulence may be present, say at a Reynolds number of 500, which would not be predicted from a simple pipe flow analogy. From measurements in a plastinated nose model, Fodil et al. [4] used a pressure-drop (loss coefficient) adjustment proportional to $Re^{-0.571}$ for Re<390 albeit they seem to attribute no physical significance to this requirement. Also, in a computational fluid dynamics (CFD) simulation, Zamankhan et al. [5] provide an equation for a variable friction factor for Re<500 which can be shown to be proportional to $Re^{-0.75}$. More recently, and using separate variable coefficients for the nasal valve and turbinate region, O'Neill and Tolley [6] were able to show a much better fit to experimental results (rhinomanometry) than for the case where the coefficients were held constant.

Figure 1 shows typical calibration curves for Venturi meter, orifice tube (cylindrical choke) and orifice plate. For specific data refer to references [7-15]. The large variation in the discharge coefficient at low Reynolds numbers for each device is clearly evident. Industrial flowmeters typically operate at high Reynolds numbers (Re >> 10^3) where the discharge coefficient (Cd) remains reasonably constant. In contrast, the Reynolds number during nasal breathing varies continuously within an approximate range of $0<Re<2\times10^3$. Assuming some degree of similarity between the characteristics of the above devices and the nose, the variation in the flow coefficient(s) throughout the nasal breathing cycle is an important consideration.

Whilst it may be tempting to apply the data of Figure 1 directly to nasal airflow, there are additional influences at play which indicate that a more accurate relationship, specific to the nose, is required. Firstly, flowmeters are calibrated during steady-state operation (constant flowrate) and secondly, the meter is located in a long length of straight pipe which approximates to fully-de-

Table 1. Information for flow coefficient of Venturi meter, orifice-plate, orifice-tube and nasal valve.

Author(s)	Device	Cd Equation	Slope $\frac{d(Cd)}{dR_e}$
Johansen [7]	Orifice Plate	Flow visualisation by dye injection upstream. At Re<10, Cd α $Re^{0.5}$ At Re>200: - Downstream vortex rings. At Re>1200: - Vortices dissipated by 'violent' turbulence. At Re>2000: - Complete turbulence	At Re< 10 $\frac{d(C_d)}{dR_e}$ $\alpha Re^{-0.5}$ thus, as Re $\rightarrow$ 0, slope $\rightarrow \infty$ At Re> 2000 $\frac{d(C_d)}{dR_e} \approx 0$
Hibi et al. [10]	Orifice Tube	$C_d = \frac{1}{(1 + 5.35\,\sigma^{-0.5})}$ where σ = 0.89 Re × (Diameter/Length)	$\frac{5.67}{Re^{0.5}(Re^{0.5}+11.34)^2}$ $\left(for\ \frac{Diameter}{Length} = \frac{1}{4}\right)$
Arun et al. [15]	Venturi	$C_d = 0.995\left(\frac{1}{1+\frac{192}{Re}}\right)^{1/2}$	$\frac{96}{Re^{0.5}(Re+192)^{1.5}}$
O'Neill and Tolley [6]	Nasal Valve	$C_d = \frac{L}{1+exp(-k\times10^{-3}R_e)} - srt$ where L = 0.68; k = 0.55 and srt = 0.1	$\frac{3.74\times10^{-4}\,exp(-0.55\times10^{-3}Re)}{\{exp(-0.55\times10^{-3}Re)+1\}^2}$

veloped flow conditions upstream. Neither of these conditions is met for the case of airflow through the major resistive segments within the nose. Because of the more complex flow conditions, it might well be argued that the flow characteristics for the nose, whilst reflecting the effects of transitional flow within the range of low to moderate Reynolds numbers, should deviate somewhat from those for a flowmeter. In the material which follows we will endeavour to show that this is indeed the case and, in particular, illustrate how the variable discharge coefficient for the nasal valve (and the variable loss coefficient for the turbinate region) can be modelled by the use of the Logistic (and tanh) function. In addition, a loss coefficient for the whole (unilateral) nose is presented which is used to provide an approximation to the critical Reynolds number (Re_{crit}).

Materials and methods

For the nasal valve

For the purpose of this study existing information for flow through Venturi, orifice-plate and orifice-tube devices was used as a comparison to the flow characteristics for the nasal valve; the latter being obtained from the mathematical model of O'Neill and Tolley [6]. The studies used for this comparison are listed in Table 1 together with analytical expressions for the discharge coefficient -v- Reynolds number. For the valve the expression is a modified form of the Logistic function. This, we found, provided a more flexible and better fit to the rhinomanometric experimental data than was the case for alternatives such as the 2K, two-coefficients method described by Hooper [16]. For each device in Table 1, the expression for the discharge coefficient was differentiated with respect to the Reynolds number in order to evaluate the likely prevailing flow conditions between mainly laminar (where the slope d(Cd)/dRe has a high value) and turbulent (where the slope d(Cd)/dRe is close to zero). This may be explained as follows:

As shown by Johansen [7] and others [11,17], studying orifice flow at very low Reynolds numbers (Re<10) the discharge coefficient is proportional to the square root of the Reynolds number i.e. Cd α $Re^{0.5}$, and so the differential d(Cd)/dRe α $Re^{-0.5}$. Thus, as Re → 0, d(Cd)/dRe → ∞. At high Reynolds numbers Cd is approximately constant, and so d(Cd)/dRe ~ 0. Thus, over the range of low to high Reynolds numbers, the magnitude of the slope d(Cd)/dRe varies from a high value to a value close to zero. Comparing this relationship for the nasal valve to those for the flow devices listed above gives some insight of the flow conditions prevailing for the valve.

*The expression is often referred to as Rohrer's equation [18]. However, the equation (in slightly different forms) has a longer history than most researchers might be aware. Gaspard Prony's polynomial equation was used by 19th century hydraulic engineers in the design of city water supplies. Henry Darcy improved upon this with a publication which accommodated the effect of pipe roughness [19].

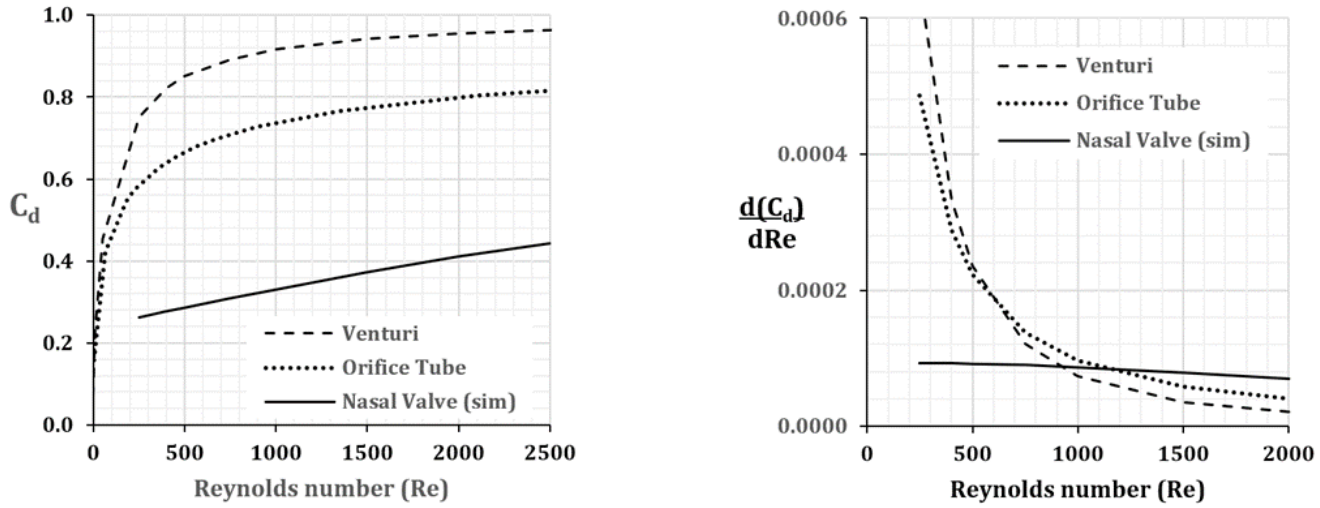

Figure 2. A) Graphical representation of data from Table 1. Coefficient of discharge Cd -v- Reynolds number for Venturi meter [15], orifice tube [10] and nasal valve [6]. B) Graphical representation of data from Table 1. Slope, d(Cd)/dRe for the devices and nasal valve shown in Figure 2A.

For the turbinate region

Whereas a coefficient of discharge (C_d) is commonly used for Venturi and orifice flow, we modelled the flow-v-pressure relationship of the turbinate region by an analogy with 'minor' (local) losses in pipe flow. Here, $K_{L\text{-turbinate}}$ is an empirically determined loss coefficient used to account for the pressure drop from the complex flow through the localised resistance. As described previously [6], we first modelled a coefficient of discharge for the turbinate region ($C_{d\text{-turbinate}}$) by a method of trial and error using the tanh function. This was then converted to a loss coefficient $K_{L\text{-turbinate}}$ using the relationship between the flow through an orifice (or orifice tube) and the Darcy-Weisbach equation applied to the case of minor losses such that

$K_{L\text{-turbinate}} = (C_{d\text{-turbinate}})^{-2}$

The relationship is:

$$K_{L-turbinate} = [ST + \{mag \times \tanh(R_e^{0.5} \times Adj)\}]^{-2}$$

where $ST = 0.043$; $mag = 0.20$ and $Adj = 0.029$.

For the whole (unilateral) nose

Representing the rhinomanometric flowrate-v-pressure difference by a second degree polynomial equation of the form

$$\Delta p = \lambda \dot{Q} + \xi \dot{Q}^2 \quad (1)^*$$

and the equation for a local pressure loss by

$$\Delta p = K_{L-nose} \cdot \rho \frac{u^2}{2} \quad (2)$$

The continuity equation is $\dot{Q} = uA$ (3)

and Reynolds number $Re = \frac{\rho u A^{1/2}}{\mu}$ (4)

where the square root of the cross-sectional flow area is used as the hydraulic diameter [6,20,21].

Equating (1) and (2) and utilizing the relationships in (3) and (4) gives the loss coefficient:

$$K_{L-nose} = \lambda \frac{2A^{3/2}}{\mu Re} + \xi \frac{2A^2}{\rho} \quad (5)$$

The relationship is the sum of two asymptotes. At high Reynolds numbers the first term on the right-hand side is negligible and the second (constant) term represents the inertial-turbulent asymptote. At low Reynolds numbers the first term predominates representing the (variable) viscous-laminar asymptote. Some researchers involved with the analysis of flow through valves and similar resistive components consider the intersection of the two asymptotes to be the location of the critical Reynolds number i.e. the region of laminar-turbulent transition. Others consider this estimate to be too high and use a value based upon the initial departure from the laminar asymptote [22]. The value for the critical Reynolds number can also be obtained directly from Eqn (5) by equating the two asymptotes and re-arranging so that

$$Re_{crit} = \frac{\lambda}{\xi}\left(\frac{1}{v\, A^{0.5}}\right) \quad (6)$$

where $v = \frac{\mu}{\rho}$

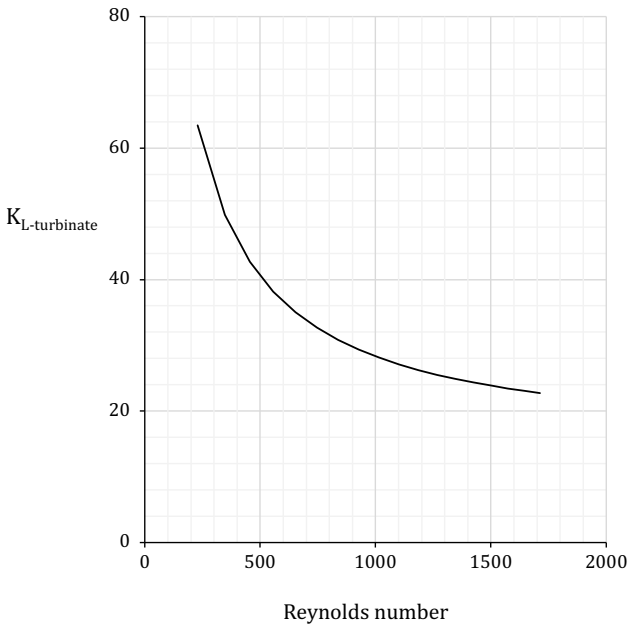

Figure 3. Turbinate region loss coefficient ($K_{L\text{-turbinate}}$) -v- Reynolds number (Re).

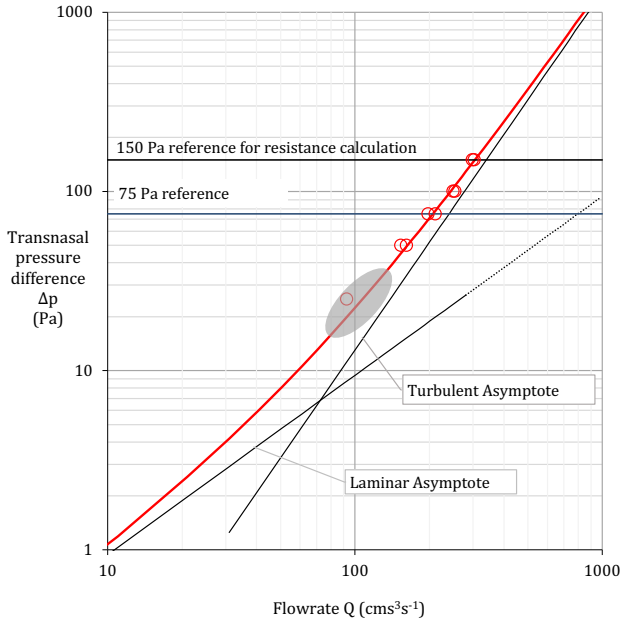

Figure 4. Rhinomanometry. Circles: experimental results in normal subjects (no decongestion): meta-analysis (O'Neill and Tolley [6]. Solid curve (red): polynomial curve fit $\Delta p=\lambda \dot{Q} +\xi \dot{Q}^2$. Straight solid lines: laminar asymptote $\Delta p=\lambda \dot{Q}$; Turbulent asymptote $\Delta p = \xi \dot{Q}^2$. Shaded oval: approximate region of major flow during normal inspiration (one nasal cavity).

Results

Nasal valve

In Figure 2A it is evident that the flow resistance of the nasal valve is considerably greater than that for both a Venturi meter and an orifice tube. For the valve, the discharge coefficient at a Reynolds number of 1,000 is about 0.33 compared to about 0.74 for an orifice tube and 0.9 for a Venturi meter. Figure 2B provides more of an insight of the flow conditions prevailing across the range of Reynolds numbers. At Re>1,000 the low slopes of all the devices and nasal valve indicate a turbulent flow regime. For Re <1,000 the slopes for the devices increase significantly at decreasing Reynolds numbers, consistent with reducing turbulence. However, the low slope for the nasal valve extends well below a Reynolds number of 500, implying significant turbulence or at least turbulent-like flow for much of nasal inspiration.

Turbinate region

Figure 3 shows the relationship between the turbinate region loss coefficient and the associated Reynolds number. The flow area used in the calculations is that of the turbinate region (144 mm^2) since, unlike industrial meter applications, there is no distal upstream (usually smaller) flow area to use as a reference. One possibility is the nasal valve dimension which, if used, would move the $K_{L\text{-turbinate}}$ curve vertically downwards.

Table 2. Effect on the calculation of the critical Reynolds number (Eqn 6) by assuming different cross sectional flow areas. 60 mm^2 is the flow area based upon the nasal valve and 140 mm^2 that based upon the turbinate region.

Flow area A (mm^2)	Critical Reynolds no. R_{crit}
60	573
100	444
140	375

Whole (unilateral) nose

Figure 4 shows rhinomanometry flowrate -v- pressure difference data and a polynomial curve fit as described by Eqn (1) [Methods]. When Δp and $\dot{Q}$ are expressed in units of Pa and m^3s^{-1}, respectively, then $\lambda = 85.2\times10^3$ and $\xi = 1.28\times10^9$. Note that flowrate is plotted on the abscissa and both axes are logarithmic. The graph has been extended well beyond the normal physiological range simply to illustrate the relationship of the fitted polynomial to the turbulent asymptote. Nasal resistance ($\Delta p/\dot{Q}$) is usually calculated using a reference pressure difference of 150 Pa (sometimes 75 Pa). The location for the region of major flow during inspiration (shaded oval) is based upon a respiration minute volume of 3 Lt. min^{-1} (one cavity) and a respiration rate of 12 min^{-1}. As the graph illustrates, reference pressures and normal respiration flowrates are displaced well away from the laminar asymptote. The relationship between the loss coefficient and Reynolds number as evaluated according to Eqn (5) is shown graphically in Figure 5. The flow area used in the calculations is 100 mm^2 which is a compromise between that for the turbinate region (~ 140 mm^2) and that for the nasal

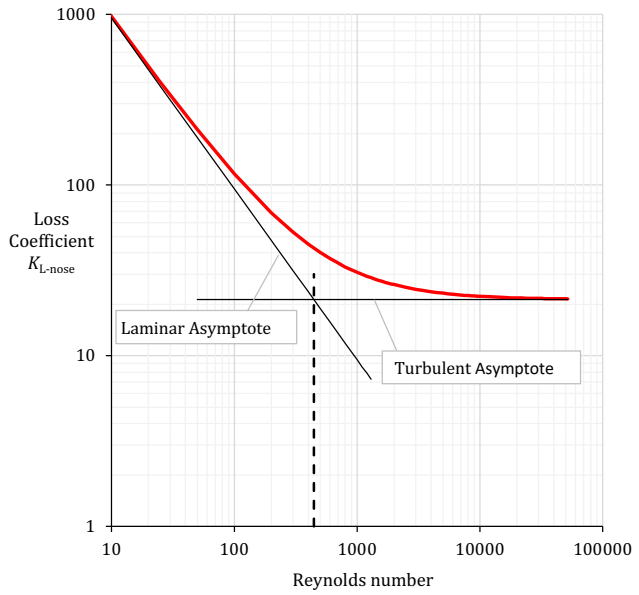

Figure 5. Loss coefficient for whole (unilateral) nose. Solid curve: loss coefficient variation as a function of the Reynolds number. Straight solid lines: laminar asymptote (inclined) $K_L = (\lambda 2A^{1.5})/\mu\,Re$; Turbulent asymptote (horizontal) $K_L = \xi 2A^2/\rho$; The Reynolds number at which the asymptotes intersect is usually taken as the critical value (Re_{crit}) i.e. laminar-turbulent transition.

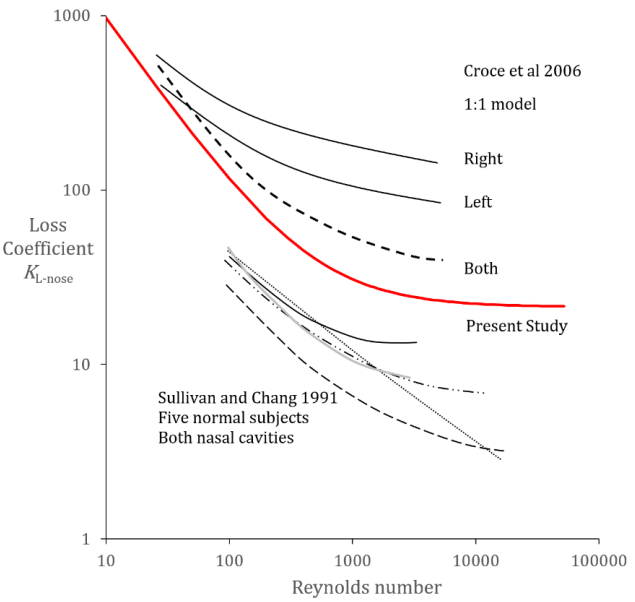

Figure 6. Loss coefficient -v- Reynolds number. Comparison of experimental results with the analysis from this present study. Croce et al. [30]: 1:1 model (~equivalent to decongested nose). Their raw data are, for convenience, shown here as single lines. Sullivan and Chang [31]: shown is their curve-fit for each of five subjects.

valve (~ 60 mm^2). There is increasing divergence from the laminar asymptote noticeable from quite low Reynolds numbers. The two asymptotes intersect at a Reynolds number of about 450 which may be taken as an estimate of the critical Reynolds number. The variation in the critical Reynolds number by assuming different flow areas is shown in Table 2.

Discussion

Within the nose there are two distinct resistive components – the nasal valve region, situated anteriorly with a minimum cross-sectional area of about 60 mm^2, and the main nasal cavity (turbinate region) with a flow area of about 140 mm^2. These dimensions result in a Reynolds number, during quiet breathing, reaching about 1000 for the valve and 600 for the turbinate region. This study has shown that the flow resistance of the nasal valve is significantly greater than that for orifice flow for which Johansen [7] reports significant turbulence observable at a Reynolds number of 1,200. Also, regarding physiological flows in otherwise normal vasculature, there is evidence that localised lesions (stenosis/aneurysm), which disrupt the flow, significantly reduce the critical Reynolds number to within the range of about $100<Re_{crit}<1{,}000$ [23-25]. In this present study, the critical Reynolds number for the whole (unilateral) nose was estimated to be 450 – comparable to Re_{crit} reported for a range of valves, orifices and nozzles [26-28]. Interestingly, Schreck et al. [29], experimenting with a 3:1 scale physical nasal model, report a transition to turbulence at a Reynolds number of approximately 600. Examination of the experimental results in the 1:1 scale physical model of Croce et al. [30] indicates a similar result. Also, Sullivan and Chang [31] obtained rhinomanometric data from five healthy adults subjected to an externally controlled flow. Their Figure 3 shows the dimensional pressure loss as a function of the Reynolds number. A comparison of these experimental results with the analysis from this present study is shown in Figure 6. The considerable difference in the vertical displacement between the studies can be explained largely by the different reference dimensions used in the flow calculations. Whereas Croce et al. [30] used a diameter of 2.48 cms taken from the connection tube, Sullivan and Chang [31] used a hydraulic diameter (8 mm - median) based upon the area of the nostril. Regarding the shapes of the curves there is considerable similarity to the loss coefficient obtained from this present study which is based upon a meta-analysis of rhinomanometric data. Arguably, this represents the most accurate nasal loss coefficient data to date. During inspiration, the disturbance of flow through the nasal valve constitutes a proximate upstream disturbance to the flow through the turbinate region. Thus, although the turbinate region's Reynolds number is well within the limits for laminar flow through straight tubes, in reality the flow is of a far more complex nature. It should also be borne in mind that the maximum rate of heat transfer to the inspired air takes place anteriorly i.e. where the air-mucosal boundary temperature difference is

Table 3. Cross-sectional area of the nasal valve from different studies. Values reported for both nasal cavities have been halved for comparison purposes. CT, computerised tomography; MRI, magnetic resonance imaging; AR, acoustic rhinometry.

	Wen et al. [42]	Subramaniam et al. [51]	Cheng et al. [52]	Keyhani et al. [53]	Garcia et al. [36]	O'Neill and Tolley [6] meta-analysis (single cavity)	
Method	CT	MRI	MRI	CT	MRI		AR decongested
Valve area (mm^2)	70	80	95	102	110	61	73

maximum [32,33]. Given that normal nasal breathing is almost effortless and provides the required mass flow at the appropriate temperature and humidity for the lower airway, it is justifiable to view the process as an example of system optimisation. Here, there is an inverse relationship between thermal resistance and flow resistance (respiratory effort) [34,35]. An important parameter regarding the effectiveness of heat and mass transfer processes is the 'surface area density' (β or SA:V) which is the ratio of surface area to volume. When expressed in units of m^2 and m^3, the value for the nose is about 1,000 [36] which compares well with the definition of a compact heat exchanger where $\beta > 700$ [37]. For the human lung β is ≈20,000 [38]. Undoubtedly, the nature of flow through the nasal valve region plays a vital role in this heat and mass transfer process.

There are clear implications for computational fluid dynamics (CFD) modelling where either the entire nasal airflow is assumed to be laminar or a low turbulence model implemented [39]. It is remarkable that the results from some turbulence models are not significantly different than those from a laminar flow model [40]. However, CFD modelling often predicts a very low transnasal pressure drop and hence a significant difference in nasal resistance values compared to rhinomanometry even when allowance is made regarding the higher reference pressure in the latter [41-44]. It is notable that cross-sectional areas for the nasal valve obtained from MRI and CT in several nasal flow studies are considerably larger than the average obtained by acoustic rhinometry (Table 3). The importance of the segmentation threshold has been highlighted by Cherobin et al. [43] and Zwicker et al. [44]. Also, areas obtained from imaging techniques are sensitive to the scan angle relative to the acoustic axis [45]. The low resistance values from some of the CFD studies suggest that the nasal valve area in particular has been overestimated. It follows that the true extent of turbulence which is present in-vivo is not adequately represented. In addition, there are difficulties in solving the Navier-Stokes equations for complex flows, with Wong [46] suggesting that a statistical approach may be more appropriate. Whilst a degree of turbulence is advantageous for the air conditioning function of the nose it has the potential of posing considerable difficulty for analysis by computational fluid dynamics.

Given that there has been considerable discussion and conflicting views regarding the presence of laminar or turbulent flow within the nose with studies involving physical models, mathematical models and numerical methods [29,30,47-50], this study has provided a unique alternative method of analysis. In particular, the estimate of the critical Reynold number can be obtained from rhinomanometric data and therefore has the potential for clinical use where abnormal flow is suspected such as in those cases listed at the beginning of the introduction.

Conclusion

Important insights into the characteristics of inspiratory nasal airflow have been gained by utilising variable flow coefficients for the nasal valve, turbinate region and the whole (unilateral) nose. The nasal valve promotes turbulent or turbulent-like flow which aids in effective mixing for air conditioning. The critical Reynolds number for the nose is about 450.

Authorship contribution

GO conceived and designed research; GO analyzed data; GO interpreted results of experiments; GO prepared figures; GO and NST drafted manuscript; NST edited and revised manuscript; GO and NST approved final version of manuscript.

Conflict of interest

No conflicts of interest are declared by the authors.

References

1. Warren DW. A quantitative technique for assessing nasal airway impairment. Am J Orthodontics Dentofacial Orthopedics 1984; 86 (4): 306-314.
2. O'Neill G, Tolley NS. Theoretical considerations of nasal airflow mechanics and surgical implications. Clin Otolaryngol 1988; (13): 273-277.
3. Rivron RP. Cross-sectional area as a measure of nasal resistance. Rhinology, 1990; 28 (4): 257-264.
4. Fodil R, Brugel-Ribere L, Croce C et al. Inspiratory flow in the nose: a model coupling flow and vasoerectile tissue distensibility. J Appl Physiol 2005; (98): 288-295.
5. Zamankhan P, Ahmadi G, Wang Z et al. Airflow and deposition of nan-particles in a human nasal cavity. Aerosol Sc and Tech 2006; (40): 463-476.
6. O'Neill G, Tolley NS. The Complexities of Nasal Airflow - Theory and Practice. Am J Appl Physiol 2019; 127 (5): 1215-1223.
7. Johansen FC. Flow through pipe orifices at

low Reynolds numbers. Proc R Soc 1930; Vol 126, Iss 801
8. Tuve GL, Sprenkle RE. Orifice discharge coefficients for viscous liquids. Instruments 1993; (6): 201-206, in Boyce MP Transport and storage of fluids, Section 10, Perry's chemical engineers' handbook-7th ed, 1997.
9. Idel'chik IE. Handbook of hydraulic resistance: coefficients of local resistance and of friction. 1966. nrc.gov/docs/ML1220/ML12209A041.pdf
10. Hibi A, Ichikawa T, Miyagawa S. Flow characteristics of cylindrical chokes. J Japan Hydraulics Pneumatics Soc 1971; 2 (2): 72-80, in Nakayama Y. Introduction to fluid mechanics. 2018 ISBN 978-0-08-102437-9.
11. Ni C. Numerical simulation of low Reynolds number pipe orifice flow. MSc Thesis (Mech Eng), Iowa State University, 2003.
12. Wang X, Kruis FE, McMurry PH. Aerodynamic focusing of nanoparticles: 1. Guidelines for designing aerodynamic lenses for nanoparticles. Aerosol Sc and Tech 2005; (39): 611-623.
13. Hollingshead CL Discharge Coefficient Performance of Venturi, Standard Concentric Orifice Plate, V-Cone, and Wedge Flow Meters at Small Reynolds Numbers. MSc Thesis, Utah State University, 2011
14. Tunay T. Investigation of the effects of different numerical methods on the solution of the orifice flow. Çukurova Uni J of the Faculty of Eng and Arch 2012; 27 (1): 39-51.
15. Arun R, Yogesh Kumar K J, V Seshadri. Prediction of discharge coefficient of Venturimeter at low Reynolds numbers by analytical and CFD Method. Int J Eng Tech Res 2015; 3 (5): 168-173.
16. Hooper WB. The two-K method predicts head losses in pipe fittings. Chem Eng 1981; (24): 96-100.
17. Sahin B, Ceyhan H. Numerical and experimental analysis of laminar flow through square-edged orifice with variable thickness. Trans Inst Measurement and Control 1996; 18 (4): 166-174.
18. Johnson AT. Biomechanics and exercise physiology: quantitative modeling. CRC Press, Taylor & Francis Group, 2007, p 298.
19. Brown GO. The history of the Darcy-Weisbach equation for pipe flow resistance. Environmental and Water Resources History, ASCE Civil Engineering Conference, 2002.
20. Muzychka YS. Analytical and experimental study of fluid friction and heat transfer in low Reynolds number flow heat exchangers. PhD Thesis, Uni Waterloo, Ontario, Canada, 1999.
21. Muzychka YS, Yovanovich MM. Pressure drop in laminar developing flow in non-circular ducts: a scaling and modelling approach. J Fluids Eng 131(11)111105-111105-11, 2009.
22. Pienaar VG, Slatter PT. Interpretation of experimental data for fitting losses, 12th Int Conf on Transport & Sedimentation of Solid Particles, Prague, Czech Republic, 20-24 Sept, ISBN 80-239-3465-1, pp 537-546, 2004.
23. Vétel J, Garon A, Pelletier D, Farinas M-I. Asymmetry and transition to turbulence in a smooth axisymmetric constriction. J Fluid Mech 2008; (607): 351-86.
24. Evju O, Mardal KA. On the Assumption of Laminar Flow in Physiological Flows: Cerebral Aneurysms as an Illustrative Example. In: Quarteroni A. (eds) Modeling the Heart and the Circulatory System, 2015; (14): 177-195.
25. Jain K. Transition to Turbulence in Physiological Flows: Direct Numerical Simulation of Hemodynamics in Intracranial Aneurysms and Cerebrospinal Fluid Hydrodynamics in the Spinal Canal. Dissertation (D.Eng), Faculty of Sc and Tech, Uni Siegen, Germany, 2016.
26. Fester V, Slatter P, Alderman N. Resistance Coefficients for Non-Newtonian Flows in Pipe Fittings. in Rheology, J De Vicente (ed), InTech (pub) 2012; 151-186.
27. Alvi SH, Sridharan K, Lakshmana Rao NS. Nozzle flows at low and moderate Reynolds numbers. J Ind Inst Sc 1977; 59 (5): 169-184.
28. Miller DS. Internal flow systems. Cranfield, BHRA Fluid Engineering pp102-105, 1978.
29. Schreck S, Sullivan KJ, Ho CM, Chang HK. Correlations between flow resistance and geometry in a model of the human nose. Am J Appl Physiol 1993; (75): 1767-75.
30. Croce C, Fodil R, Durand M et al. In vitro experiments and numerical simulations of airflow in realistic nasal airway geometry. Ann Biomed Eng 2006; 34 (6): 997-1007.
31. Sullivan KJ, Chang HK. Steady and oscillatory transnasal pressure-flow relationships in healthy adults. Am Physiol Soc 1991; 983-992.
32. Keck T, Leiacker R, Riechelmann H, Rettinger G. Temperature profile in the nasal cavity. Laryngoscope 2000; 110 (4): 651-654.
33. Yu S, Sun X, Liu Y. Numerical analysis of the relationship between nasal structure and its function. Sc World J 2014.
34. Bejan A. Convection heat transfer. 3rd Edition, Wiley, 2004, pp 159-160.
35. Wechsatol W, Lorente S, Bejan A. Dendritic heat convection on a disc. Int J Heat Mass Transfer 2003; 46 (23): 4381-4391.
36. Garcia GJM, Bailie N, Martins DA, Kimbell JS. Atrophic rhinitis: a CFD study of air conditioning in the nasal cavity. J Appl Physiol 2007; (103): 1082-1092.
37. Shah RK, Sekulic DP. Fundamentals of heat exchanger design. Wiley, 2003, p 8.
38. Coxson HO, Rogers RM, Whittall KP, D'Yachkova Y, Pare PD, Sciurba FC, Hogg JC. A quantification of the lung surface area in emphysema using computed tomography. Am J Resp Crit Care Med 1999; (159): 851-856.
39. Quadrio M, Pipolo C, Corti S et al. Review of computational fluid dynamics in the assessment of nasal air flow and analysis of its limitations. Eur Arch Otorhinolaryngol 2014; 271 (9): 2349-2354.
40. Aasgrav E, Johnsen SG, Simonsen AJ, Muller B. CFD simulations of turbulent flow in the human upper airways. 12th Int Conf on CFD in Oil & Gas, Met and Proc Inds. SINTEF, Trondheim, Norway, 2017.
41. Osman J, Grosmann F, Brosien K, Kertzscher U, Goubergrits L, Hildebrandt T. Assessment of nasal resistance using computational fluid dynamics. Curr Dir in Biomedical Eng 2016; 2 (1): 617-621.
42. Wen J, Inthavong K, Tian ZF, Tu JY, Xue CL, Li CG. Airflow patterns in both sides of a realistic human nasal cavity for laminar and turbulent conditions. 16th Australian Fluid Mechanics Conference, Gold Coast, 68-74; 2-7 Dec 2007.
43. Cherobin GB, Voegels RL, Gebrim EMMS, Garcia GJM. Sensitivity of nasal airflow variables computed via computational fluid dynamics to the computed tomography segmentation threshold. PLoSONE 13(11):e0207178, 2018.
44. Zwicker D, Yang K, Melchionna S, Brenner MP, Liu B, Lindsay RW. Validated reconstructions of geometries of nasal cavities from CT scans. Biomed Phys Eng Express 4 2018a.
45. Cakmak O, Coskun M, Celik H, Buyuklu F, Ozluoglu LN. Value of acoustic rhinometry for measuring nasal valve area. Laryngoscope 2003; (113): 295-302.
46. Wong B. The mathematical theory of turbulence or chaos. Int J Nonlinear Science 2010; 10 (3): 264-278.
47. Kelly JT, Prasad AK, Wexler AS. Detailed flow patterns in the nasal cavity. J Appl Physiol 2000; (89): 323-337.
48. Betlejewski S, Betlejewski A. The influence of nasal flow aerodynamics on the nasal physiology. Otolaryngol Pol 2008; 62 (3): 321-325.
49. Churchill SE, Shackelford LL, Georgi JN, Black MT. Morphological variation and airflow dynamics in the human nose. Am J Hum Biol 2004; (16): 625-638.
50. Zwicker D, Ostilla-Monico R, Lieberman DE, Brenner MP. Physical and geometric constraints shape the labyrinth-like nasal cavity. PNAS 2018b; March 20, 115 (12): 2936-2941.
51. Subramaniam RP, Richardson RB, Morgan KT, Kimbell JS, Guilmette RA. Computational fluid dynamics simulations of inspiratory airflow in the human nose and nasopharynx. Inhal Toxicol 1998; 10 (2): 91-120.
52. Cheng YS, Yeh HC, Guilmette RA et al. Nasal deposition of ultrafine particles in human volunteers and its relationship to airway geometry. Aerosol Sc and Tech 1996; 25 (3): 274-291.
53. Keyhani K, Scherer PW, Mozell MM. Numerical simulation of airflow in the human nasal cavity. J Biomech Eng 1995; 117 (4): 429-441.
54. O'Neill G, Tolley NS. The dynamics of nasal airflow. Facial Plastic Surgery 1990; 7 (4): 215-220.
55. Li C, Farag AA, Maza G et al. Investigation of the abnormal nasal aerodynamics and trigeminal functions among empty nose syndrome patients. Int Forum Allergy Rhinol 2018; 8 (3): 444-452.
56. Sommer F, Simmen D, Briner HR et al. Effects of nasal wall lateralization and pyri-

form turbinoplasty on nasal air conditioning. Otorhinolaryngol Head Neck Surg 2016; 2 (2): 1-5.
57. Papp J, Leiacker R, Keck T, Rozsasi A and Kappe T. Nasal air conditioning in patients with chronic rhinosinusitis and nasal polyposis. Arch Otolaryngol Head Neck Surg 2008; 134 (9): 931-935.

Professor N. S. Tolley, MD FRCS DLO
Dept of Otolaryngology-Head and Neck Surgery
St Mary's Hospital
Imperial College Healthcare NHS Trust
London
UK

E-mail: n.tolley@imperial.ac.uk